Applied Surface Science 559 (2021) 149835

Contents lists available at ScienceDirect

Applied Surface Science

journal homepage: www.elsevier.com/locate/apsusc

Full Length Article

Absence of spillover of hydrogen adsorbed on small palladium clusters anchored to graphene vacancies

Alejandra Granja-DelRío [a,b], Maite Alducin [c,b,*], J. Iñaki Juaristi [d,b], María J. López [a], Julio A. Alonso [a,b]

[a] Departamento de Física Teórica, Atómica y Óptica, Universidad de Valladolid, 47011 Valladolid, Spain
[b] Donostia International Physics Center (DIPC), Paseo Manuel de Lardizabal 4, 20018 Donostia-San Sebastián, Spain
[c] Centro de Física de Materiales CFM/MPC (CSIC-UPV/EHU), Paseo Manuel de Lardizabal 5, 20018 Donostia-San Sebastián, Spain
[d] Departamento de Polímeros y Materiales Avanzados: Física, Química y Tecnología, Facultad de Químicas UPV/EHU, Apartado 1072, 20080 Donostia-San Sebastián, Spain

ARTICLE INFO

Keywords:
Hydrogen spillover
Hydrogen adsorption
Hydrogen storage
Graphene vacancies
Hydrogenated Palladium
Ab initio molecular dynamics

ABSTRACT

Experimental evidence exists for the enhancement of the hydrogen storage capacity of porous carbons when these materials are doped with metal nanoparticles. One of the most studied dopants is palladium. Dissociation of the hydrogen molecules and spillover of the H atoms towards the carbon substrate has been advocated as the reason for the enhancement of the storage capacity. We have investigated this mechanism by performing ab initio density functional molecular dynamics (AIMD) simulations of the deposition of molecular hydrogen on Pd_6 clusters anchored on graphene vacancies. The clusters are initially near-saturated with atomic and molecular hydrogen. This condition would facilitate the occurrence of spillover, since our energy calculations based on density functional theory indicate that migration of preadsorbed H atoms towards the graphene substrate becomes exothermic on Pd clusters with high hydrogen coverages. However, AIMD simulations show that the H atoms prefer to intercalate and absorb within the Pd cluster rather than migrate to the carbon substrate. These results reveal that high activation barriers exist preventing the spillover of hydrogen from the anchored Pd clusters to the carbon substrate.

1. Introduction

In the current search for clean fuels for transportation that could replace gasoline, hydrogen stands out as a promising one [1–3]. The electrical engine in the hydrogen cars is a fuel cell [4] in which hydrogen coming from the storage tank reacts with atmospheric oxygen producing an electric current, and the only emission product from the reaction is water. Hydrogen can be easily produced by different methods, including the electrolysis of water. The technology of hydrogen fuel cells is well developed [4], and the recharging times of the present hydrogen cars are substantially smaller than the recharging times for the electric battery cars. However, the main challenge that has to be met to achieve a successful hydrogen transportation economy is an efficient storage of hydrogen on board [5]. The only storage method currently in use consists in storing hydrogen gas at high pressure (about 700 atm) in a container. This is already an important advance, but in the opinion of many scientists and engineers it is not the ultimate solution, in part because of safety reasons. This has motivated the investigation of alternative storage technologies, and one that is receiving a lot of attention is the storage of hydrogen in porous and layered materials. Different classes of porous and layered materials have been studied: porous carbons [6–10], metal organic frameworks [11], zeolites [12], clathrate hydrates [13], microporous organic polymers [14] or WS_2 nanoparticles and nanotubes [15,16], among others.

There is increasing interest in the storage of hydrogen in porous carbon materials, which have low weight and a large specific surface area. Both experiments [7] and computer simulations [6,8,9] indicate that porous carbons do not adsorb enough hydrogen to fulfill the required technological targets. Experiments, however, reveal an enhancement of the storage capacity when porous carbons, carbon nanotubes and carbon fibers are doped with metal clusters and nanoparticles [17–33]. Non-transition [17–20] and transition metal

* Corresponding author at: Centro de Física de Materiales CFM/MPC (CSIC-UPV/EHU), Paseo Manuel de Lardizabal 5, 20018 Donostia-San Sebastián, Spain.
E-mail addresses: alejandra.granja@uva.es (A. Granja-DelRío), maite.alducin@ehu.eus (M. Alducin), josebainaki.juaristi@ehu.eus (J.I. Juaristi), maria.lopez@fta.uva.es (M.J. López), jaalonso@fta.uva.es (J.A. Alonso).

https://doi.org/10.1016/j.apsusc.2021.149835
Received 26 January 2021; Received in revised form 12 April 2021; Accepted 12 April 2021
Available online 2 May 2021

nanoparticles [20–33] have been investigated as dopants. A mechanism of spillover [34–37] has been advocated to explain the observed enhancement of the hydrogen storage capacity of these materials [21–25,35,38,39]. In the proposed spillover mechanism, molecular hydrogen is first adsorbed on the metal nanoparticle. The molecule then dissociates and the hydrogen atoms migrate and spill onto the surface of the substrate carbon material. Recent work has analyzed the spillover of hydrogen from Pt nanoparticles into metal oxide surfaces [37]. For this purpose, X-ray absorption spectro-microscopy was employed to measure the extent of reduction of iron oxide nanoparticles by the hydrogen generated in the Pt particles placed some distance away [40]. The spillover was clearly detected in the case of reducible surfaces like titanium oxide. However, spillover on the non-reducible supports like aluminum oxide is drastically reduced [37]. Some interesting experiments have also been performed in the case of carbonaceous substrates. Infrared (IR) absorption has revealed the existence of C-H bonds following the hydrogen loading of highly defective carbon nanotubes doped with palladium nanoparticles. The defects –vacancies and larger holes– were created by an oxidation pretreatment of carbon nanotubes, and the IR results were interpreted as indicating adsorption of H atoms at the defect sites after spilling from the Pd nanoparticles [22]. However, this is not the only possible source of C-H bonds. The unsaturated borders of graphene vacancies and larger holes are very reactive and can directly dissociate incoming H_2 molecules and trap the H atoms [41]. Inelastic neutron scattering experiments also found evidence of C-H bonds in Pd-doped activated carbon fibers initially loaded with hydrogen at 77 K and later subjected to a prolonged treatment at room temperature for 24 h [42]. In this case, the fraction of H_2 molecules undergoing spillover was estimated to be very small, about 1.2%. These experiments motivate the detailed atomistic study of the spillover mechanisms from Pd clusters and nanoparticles.

In a previous work we have addressed the issue of the hydrogen spillover from small transition metal nanoparticles into carbonaceous substrates from a computational point of view. For this purpose, graphene was used as a model for the substrate, because atomistic molecular dynamics simulations indicate that graphene is a good model for the pore walls of porous carbons [43,44]. Density functional molecular dynamics simulations were then performed to study the adsorption of H_2 molecules on Pd_6 and Pd_{13} supported on pristine graphene [45]. Different initial conditions, including clean Pd clusters and clusters saturated with hydrogen, were considered. The final outcomes from an extensive search of dynamical simulations were distributed among molecule rebound, molecular adsorption, and dissociative adsorption on the Pd nanoparticle. However, not a single case was detected of the H_2 molecule or the H atoms spilling from the nanoparticle over the carbon substrate, casting doubts about the validity of this mechanism for the case of palladium nanoparticles on carbonaceous substrates. In fact, calculated barriers of 2 eV or more were found preventing the spillover of H atoms.

Nonetheless, the assumption of having pristine graphene as the substrate in that work was probably too restrictive. In this respect, the simulations can be made more realistic if the metal particles are firmly anchored on substrate defects. This is expected to be the case in the experiments because surface defects prevent the diffusion of clusters through the surface [46,47]. Dissociation of H_2 on Pd clusters supported on defects of the carbonaceous surface leads to a change of the cluster structure [48], and the immediate question is whether the structural change may facilitate the spillover mechanism. Consequently, in this work we have investigated the effect of having more realistic conditions: anchoring the Pd clusters on graphene vacancies, and studying the case of highly hydrogen-covered clusters. Interestingly, we find that migration of adsorbed hydrogen to the carbon atoms located near the vacancy is exothermic by about 0.2–0.4 eV, when the cluster is covered with eight or more hydrogen molecules. Motivated by these promising results, we have performed extensive AIMD simulations that account for the whole reaction process, namely, (i) the collision of gas-phase H_2 with the cluster already covered with nine hydrogen molecules, (ii) the adsorption or reflection of the H_2 molecule and (iii) the concomitant perturbation that either the adsorbed or the reflected molecule causes on the cluster that may eventually end in the speculated spillover of one of the adsorbed hydrogen atoms. In contrast to our initial expectations however, there is a complete absence of hydrogen migration to the graphene layer in the extensive set of 600 trajectories. The analysis of the trajectories will provide meaningful insights on the reasons that prevent the occurrence of the spillover mechanism.

The paper is organized as follows. After describing the theoretical methods, we start showing the energetics of the spillover process calculated with DFT. Next, the results from the AIMD simulations performed for the cluster and the substrate initially at 0 K and at 300 K will be shown and discussed in connection with our previous results on the pristine graphene layer. The main conclusions are summarized at the end.

2. Theoretical methods

Hydrogen-covered Pd_6 clusters anchored on a graphene vacancy are studied with spin-polarized density functional theory (DFT) [49], using the VASP code [50,51]. Electronic exchange and correlation effects are described with the PW91 version of the generalized gradient approximation functional [52]. The use of this functional is motivated by our previous works showing that PW91 gives good results in similar systems [45,48,47,53,54]. The valence-core electronic interaction is treated in the projector augmented wave (PAW) approximation [55]. Specifically, we use the PAW potentials for H, C, and Pd that have one, six, and 16 valence electrons, respectively [56]. The electronic wave functions are expanded in a plane-waves basis with an energy cutoff of 400 eV. The Brillouin zone integration is performed with a Γ-centered $2 \times 2 \times 1$ Monkhorst–Pack grid of special **k**-points [57]. Fractional electronic-state occupancies are described by the first-order Methfessel–Paxton broadening scheme, with a width of 0.1 eV [58]. An energy precision of 10^{-5} eV is used for the electronic convergence. In the static DFT calculations, structural relaxations to find the lowest energy configurations are carried out until all the forces on the atoms are below 0.01 eV/Å. Large 6×6 hexagonal supercells of the single-vacancy graphene layer separated by 14 Å of vacuum along the perpendicular direction are used in all the calculations. The reason is that we are interested in studying the single vacancy graphene layer saturated with a hydrogen-covered Pd_6 cluster (in the following denoted as $n\mathrm{H}_2^*$-Pd_6@Gvac, where $*$ denotes adsorbed species and n refers to the total number of molecularly and dissociatively adsorbed H_2^*).

The adsorption dynamics of H_2 on the $9\mathrm{H}_2^*$-Pd_6@Gvac system is studied with total energy-conserving ab initio molecular dynamics (AIMD) simulations for two initial substrate temperatures, 0 and 300 K. Furthermore, it is assumed that the reaction proceeds in both cases at the zero pressure limit (i.e., one impinging gas-phase molecule per simulated AIMD trajectory). In the (constant-energy) AIMD simulations at 0 K, the Pd and C atoms of the $9\mathrm{H}_2^*$-Pd_6@Gvac substrate are initially at rest in their equilibrium positions (bottom-left image in Fig. 1). In the simulations at 300 K, the initial positions and velocities of the atoms in the substrate are randomly taken from a canonical set of configurations. The latter is generated by equilibrating the $9\mathrm{H}_2^*$-Pd_6@Gvac substrate at 300 K during 3 ps using the Nosé-Hoover thermostat [59] implemented in VASP. Let us remark that the use of constant-energy AIMD simulations with an appropriate set of initial positions and velocities is a reasonable approximation to account for substrate temperature effects during the first initial ps of interest (4 ps in our case) [60]. This is the standard procedure used in present gas-surface dynamics studies [61–64,60,65–67].

All the (constant-energy) AIMD trajectories are integrated up to 4 ps using a time step of 0.5 fs. The H_2 molecule starts with its center of mass (CM) located at a distance $Z = 9$ Å from the graphene layer and impinges

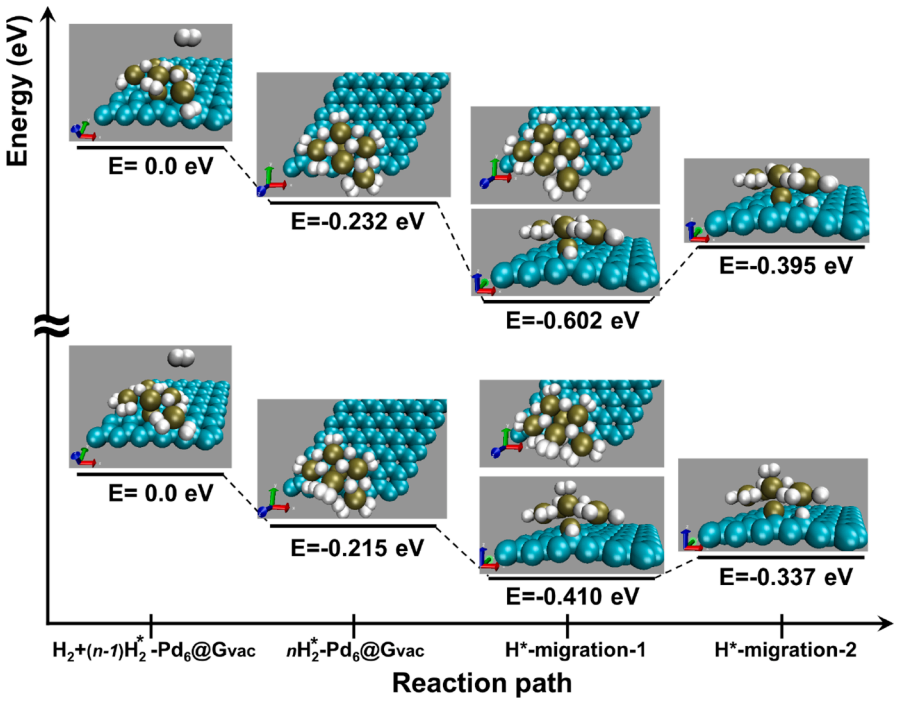

Fig. 1. DFT energy diagram of H* migration on single-vacancy graphene saturated with the $9H_2^*$-Pd_6 cluster (top) and the $10H_2^*$-Pd_6 cluster (bottom). Energies in each diagram are referred to the configuration conformed by the gas-phase H_2 located 9 Å from the graphene layer with the equilibrium bond length (0.75 Å) and the optimized $(n-1)H_2^*$-Pd_6@Gvac substrate. In each image, C, Pd, and H atoms are represented by blue, brown, and white spheres.

perpendicular to it with E_i=0.125 eV and $E_{vib}(\nu = 0, j = 0)$=0.27 eV as initial translational and vibrational energies, respectively. Finally, the molecular orientation and the CM position over the graphene layer (X, Y) are randomly sampled, although the (X, Y)-sampling is restricted to the area of the simulation cell containing the $9H_2^*$-Pd_6 cluster in order to optimize the computational effort. Similar incidence conditions were used in Ref. [45] that will facilitate the comparison to the case of the cluster being adsorbed on the pristine graphene layer.

During the time spanned by each simulated trajectory the impinging H_2 may bounce back towards vacuum (reflection) or be (molecularly) adsorbed on the $9H_2^*$-Pd_6@Gvac cluster. In practice, a trajectory is counted as reflected if either H_2 reaches the initial height of 9 Å with positive normal translational momentum or it exits the (6 × 6) parallelogram centered at the instantaneous geometrical center of the $9H_2^*$-Pd_6@Gvac cluster. The latter condition is imposed to restrict the study to the single cluster case of our interest. Dissociation of either the incoming gas-phase H_2 or any of the preadsorbed H_2^* is not observed. Interestingly, at $T_s = 300$ K, both the adsorption and reflection of the impinging H_2 can cause desorption of H_2^* molecules from the $9H_2^*$-Pd_6@Gvac cluster, as it will be discussed below.

3. Static DFT calculations for H-covered Pd_6 clusters anchored on graphene surfaces

In contrast to the case of low coverage, our static DFT calculations for nH_2^*-Pd_6@Gvac with coverages $n = 8$, 9, and 10 show that H* migration from the Pd_6@Gvac cluster towards the carbon substrate becomes energetically favored on these highly H-covered clusters. More specifically, migration to the carbon atoms nearest to the vacancy is exothermic by 0.175, 0.370, and 0.195 eV for $n = 8$, 9 and 10, respectively. Fig. 1 summarizes the results for the clusters covered with nine and ten H_2 molecules. For each coverage, the figure shows the basic configurations that would describe the spillover process, namely, (i) adsorption of one H_2 molecule on $(n-1)H_2^*$-Pd_6@Gvac that completes the nominal coverage n, (ii) migration of one H* atom from its initial chemisorbed position on the Pd_6 surface to one of the nearest C atoms bound to the Pd atom at the bottom apex of the cluster, and (iii) migration of this H* to a nearby C atom not bound to either the Pd apex or the vacancy. In all the relaxed configurations, the structure of the Pd cluster is an incomplete pentagonal bipyramid (IPB). In that structure, the Pd atom at the bottom apex of the bipyramid is directly bound to the three C atoms nearest to the vacancy center, which are the C atoms with dangling bonds. As shown recently [48], IPB is the lowest energy configuration of Pd_6 supported on Gvac with one dissociatively adsorbed hydrogen molecule on the Pd_6 cluster. The same IPB structure is retained for Pd_6@Gvac with different hydrogen coverages [53]. According to our calculations at several coverages and in agreement with previous studies [53], a maximum of three molecules can be dissociatively adsorbed on the IPB Pd_6@Gvac, but the cluster can additionally adsorb up to seven more H_2 molecules. Hence, $n = 10$ corresponds to the saturation coverage.

Fig. 1 shows that completion of H-coverages $n = 9$ and $n = 10$ in the zero-pressure limit liberates about 0.2 eV. In the quasi-saturated cluster ($n = 9$), H_2^* molecules and H* atoms bind to the five upper Pd atoms in a rather symmetrical fashion. Addition of the 10th molecule hardly alters the $9H_2^*$-Pd_6@Gvac configuration because the new molecule adsorbs on the free adsorption site that exists on the topmost Pd atom (compare the second image of each energy diagram in Fig. 1). Remarkably, migration of any of the H* atoms to the C atoms nearest to the vacancy (this step is labelled H*-migration-1 in the figure) is exothermic by 0.370 and 0.195 eV on the $9H_2^*$- and $10H_2^*$-Pd_6@Gvac clusters, respectively. The exothermicity is independent of which particular H* migrates because in all cases the remaining adsorbates rearrange and end up in the same relaxed configuration (third image in each energy diagram). From this point, the next step that would represent the beginning of the migration on the graphene layer (H*-migration-2) becomes endothermic by about 200 meV on the quasi-saturated cluster, but less than 100 meV are necessary on the saturated one. Yet, the whole process is energetically favored from the perspective of the adsorbing H_2 (-0.395 and -0.337 eV on the quasi-saturated and saturated clusters, respectively).

This is a very promising result that sharply contrasts with the case in which the Pd clusters are adsorbed on pristine non-defective graphene. In the latter case the spillover process is highly endothermic, with spillover energies of about 1.8 eV and 2 eV per H atom for spillover from Pd_6 and Pd_{13} [45], respectively. Instead, when the dopant Pd cluster is anchored on a graphene vacancy the spillover would be energetically possible. However, the existence of activation barriers may interfere with this expectation, and in the next section we report the results of ab initio molecular dynamics simulations which analyze this issue in detail.

4. AIMD simulations of H_2 impinging on H-quasi-saturated Pd_6 clusters anchored on graphene surfaces

The above DFT results showing that the H*-migration steps become exothermic on the highly H-covered Pd_6 clusters are very promising in our aim to understand the mechanisms that favor the adsorption of hydrogen on graphene-based materials doped with metal nanoparticles [17–33]. However, the existence of energy barriers, as well as the characteristics of the configurational space along the reaction paths are also crucial properties controlling the efficiency and likelihood of the process. Aimed at exploring these additional ingredients, we perform a series of AIMD simulations on the adsorption dynamics of H_2 colliding on the quasi-saturated $9H_2^*$-Pd_6 cluster. Specifically, a set of 500 constant-energy AIMD trajectories are calculated with the substrate ($9H_2^*$-Pd_6@Gvac) initially at $T_s = 0$ K. Among other features, these extensive AIMD simulations will allow us to explore the configurational space leading from H_2 adsorption to H*-migration to positions on top of C atoms nearest to the vacancy (and eventually to the energetically less favored migration to more distant C atoms on the graphene layer). Finally, a second set of 100 constant-energy AIMD trajectories that are calculated for H_2 impinging on the substrate at $T_s = 300$ K provide additional insights on the feasibility of H*-migration under ambient temperature conditions.

The trajectories leading to the adsorption of the impinging H_2 molecule on $9H_2^*$-Pd_6@Gvac provide information about the possibility of H spillover from the fully H-saturared system, $10H_2^*$-Pd_6@Gvac, towards the supporting graphene layer. However, as shown below, a substantial number of trajectories do not lead to adsorption but to rebounding of the gas-phase H_2 molecule. These H_2 reflected trajectories are also relevant because, although indirectly, provide information –at none additional computational cost– on the dynamics and the likeliness of the spillover process on the quasi-saturated system. Recall that, according to our static DFT calculations, the spillover is also an exothermic process in the $9H_2^*$-Pd_6@Gvac system.

4.1. 0.125 eV-H_2 impinging on $9H_2^*$-Pd_6@Gvac at 0 K

Adsorption of H_2 on the quasi-saturated cluster occurs in only 11 out of 500 trajectories. The rest are scattered back to vacuum after bouncing against the cluster or the graphene layer (scattering trajectories). These numbers suggest that saturating the cluster with hydrogen is a rather unlikely process in the low pressure limit because there is only one free available adsorption site. A quick look at the initial (X, Y) positions of the impinging H_2 shows that the molecules must attack the cluster very close to this available free spot. However, this condition is not sufficient to assure successful H_2 adsorption, since there are also trajectories that starting above this spot end up as reflected.

Irrespective of being adsorbed or reflected, the collision of H_2 with the $9H_2^*$-Pd_6 cluster causes the mobility of the adsorbed H* atoms and H_2^* molecules, but without desorbing them. As a result, there is a certain deformation of the Pd cluster, which adapts to the mobile adsorbates while remaining firmly anchored to the vacancy through the Pd atom at the lower end of the axis of the bipyramid. Focusing on the adsorbing trajectories–of interest for understanding the H* migration mechanisms upon hydrogen saturation,– there are two cases for which the Pd cluster undergoes a strong structural change (bent-cluster trajectories), with one of the five upper Pd atoms shifting upwards and causing the deformation from the initial incomplete pentagon to a concave bent conformation that facilitates the intercalation of the adsorbed H* atoms between the Pd atoms. The snapshots for one of these two trajectories shown in the bottom panels of Fig. 2 provide a clear picture of the deformation. The structural transformation from IPB to the bent structure does not take place immediately upon adsorption of the H_2 molecule, but it requires some time for the energy to redistribute in the cluster and channel into the suitable modes leading to the structural change. Thus the cluster starts to bend about 1.9 ps after the initial collision, that occurs at $t \simeq 75$ fs in our simulations. Similar time delays have been observed in structural transformations of Pd_6@Gvac induced by the dissociative adsorption of hydrogen [48]. The IPB structure is basically kept in the rest of the adsorbing trajectories (nine), although the cluster might slightly rotate around the axis perpendicular to the graphene layer or exhibit a more planar and open structure (i.e., larger internuclear distances between the Pd atoms in the pentagon) depending on each particular trajectory.

The perturbation caused by the impinging H_2 can be considered as very minor in five of these nine trajectories that preserve the IPB structure, since the adsorbates, although vibrationally (H_2^* also rotationally) excited, remain in their original adsorption positions. Thus, the nascent saturated cluster forms and stays on the stable IPB $10H_2^*$-Pd_6 configuration found in the static DFT calculations discussed above. The snapshots shown in Fig. 2 (top) for one trajectory of this kind (called soft adsorption in the following) are very descriptive of the minor perturbation caused by the adsorption process. Note, for instance, that the arrangement of H* and Pd atoms in each snapshot is very similar to the relaxed IPB $10H_2^*$-Pd_6 configuration of Fig. 1. Also, the time evolution of the H* heights plotted in Fig. 3 (left bottom panel) shows in detail that the adsorbates basically remain at their positions during the first 4 ps upon H_2 adsorption.

Regarding the possible migration of H* atoms towards the vacancy-neighbor C atoms, we observe that H_2 adsorption is accompanied by the displacement of one (or even two) H* atoms to closer distances to the graphene layer in the remaining four trajectories that preserve the IPB structure. However, in none of these cases the H* adsorbate is able to approach to distances less than 2.5 Å from the layer. A closer inspection of these trajectories reveals that the H* adsorbate becomes in fact embedded in the cluster and still far from the vacancy-neighbor C atoms, i. e., far from the position that occupies in the H*-migration-1 configuration shown in Fig. 1. We qualify this kind of downwards displacement as frustrated migration because the mobile H* atoms, staying at substantial distances from the graphene layer, are not forming the expected C-H* bonds. The heights plotted in Fig. 3 for one of these H*-embedding trajectories show that two adsorbates, H*(1) and H*(2) (black and red H* in the figure), reach heights of 2.7–3 Å. The displacement is particularly large for H*(1), that descends around 1.5 Å during the interval lasting from 0.9 to 1.5 ps. The corresponding snapshots in Fig. 2 (middle panels) illustrate in detail the frustrated migration paths followed by H*(1) and H*(2). In particular, note that H*(1) moves first over the external bridge position instead of descending directly through the hollow site–as it is in fact observed in other H*-embedding trajectories (not shown)–. Interestingly, the H*(1) frustrated migration is accompanied by the displacement of the H*(6) atom (colored in blue) towards the empty adsorption site that H*(1) left behind, and stays oscillating above the in-between bridge position. Thus, the arrangement adopted by the topmost H* adsorbates resembles that of the H*-migration-1 step depicted in Fig. 1, even if H*(6) is not directly involved in the frustrated migration. The fact that H*(6) remains on the upper face of the cluster in all the 500 AIMD trajectories suggests the existence of large energy barriers that prevent the spillover of this particular adsorbate atom.

Similar kinds of frustrated migrations occur in the two bent-$10H_2^*$-Pd_6 trajectories with one of the upper H* atoms going down to heights of

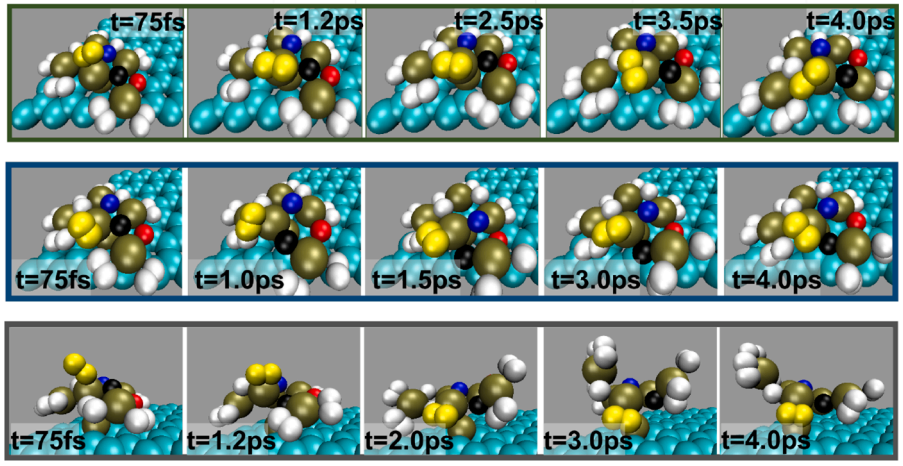

Fig. 2. Representative snapshots of the three types of adsorbing AIMD trajectories that were identified for H_2 impinging on $9H_2^*$-Pd_6@Gvac at $T_s = 0$ K. Top panels: soft-adsorption. Middle panels: H*-embedding. Bottom panels: bent-cluster. Time interval indicated in each panel. Blue and brown spheres represent C and Pd atoms, respectively. H atoms are in white, except for the adsorbing H_2 (yellow) and the three adsorbates relevant to follow the frustrated H*-migration, namely, H*(1) (black), H*(2) (red), and H*(6) (blue). (For interpretation of the references to colour in this figure legend, the reader is referred to the web version of this article.)

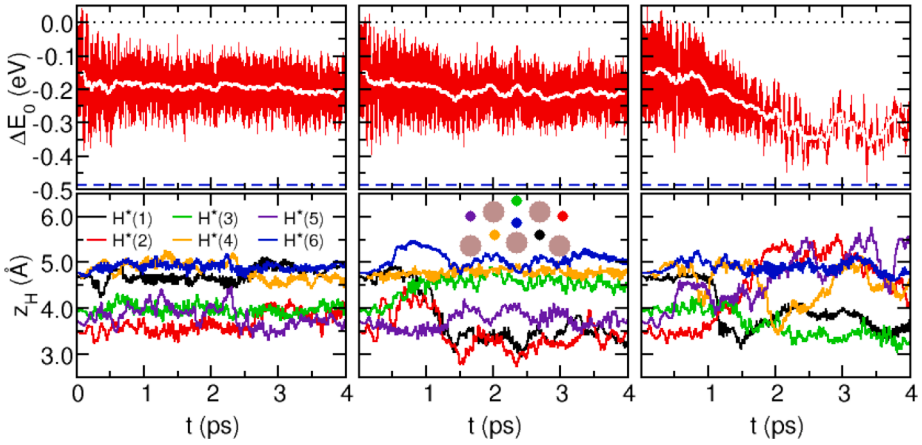

Fig. 3. Time evolution of the potential energy change ΔE_0 (top panels) and the H* heights from the graphene layer z_H (bottom panels) for each of the representative adsorbing trajectories shown in Fig. 2: soft-adsorption (left), H*-embedding (middle), and bent-cluster (right). Top view of the initial positions of each H* are depicted in the inset using the same color code of the z_H curves. The white and blue-dashed curves in the top panels show the time-average of ΔE_0 calculated in intervals of ± 0.1 ps and the potential energy of $10H_2^*$-Pd_6@Gvac referred to the gas-phase H_2 with the ZPE correction (0.270 eV), respectively.

around 3 Å, that are still far from the graphene layer. Motivated by these results, we have performed additional DFT static calculations to further characterize the energetics of the H* migration process in the bent $10H_2^*$-Pd_6@Gvac cluster. We have found that for every single H*, migration from its optimized chemisorbed position on the bent cluster to one of the nearest C atoms of the graphene layer is endothermic. This behaviour is in contrast with the exothermic H* migration from the IPB structure shown in the lower panel of Fig. 1, although the energy cost for migration of H*(4) and H*(5) from the bent-$10H_2^*$-Pd_6 structure to the graphene layer is of only a few tens of meVs.

Turning to the reflected trajectories, the perturbation that the incoming H_2 molecule creates on the $9H_2^*$-Pd_6@Gvac cluster causes the mobility of all the adsorbates. However, there is no trace of H* migration in any of the 489 trajectories. In view of all the above analysis, we conclude that H* migration on the saturated and quasi-saturated clusters, although energetically possible, is hindered by the existence of energy barriers that prevent the adsorbates breaking their bonds with the upper Pd atoms of the cluster and, hence, to access the H*-migration-1 configuration. In this respect, the analysis of the potential energy along the AIMD trajectories can provide additional information on the energy landscape that becomes accessible through the adsorption process.

The time evolution of the potential energy of the system $E_0(t)$ with respect to its value at $t = 0$, i. e., $\Delta E_0(t) = E_0(t) - E_0(0)$, is plotted in the top panels of Fig. 3 for each of the three types of adsorbing trajectories. Note that the initial oscillatory behavior of $\Delta E_0(t)$ common to all trajectories, that ranges from 0 to ≈ -0.27 eV, is simply associated to the zero point energy (ZPE) of the incoming H_2 molecule that starts at time $t = 0$ with its bond length elongated at the outer turning point in all the trajectories. As the molecule starts to interact with the substrate, the oscillations change differently on each trajectory, enclosing information not only of the change of the H_2 ZPE while adsorbed, but of all the dynamics induced on the adsorbed H* atoms, H_2^* molecules, the cluster, and also locally in the graphene layer. The fact that ΔE_0 rapidly deviates well below the $\Delta E_0 = 0$ line in all the adsorbing trajectories indicates that the adsorption of H_2 up to saturation is exothermic.

Starting with the soft adsorption trajectory, we observe that the new pronounced oscillations in ΔE_0 that develop at around 0.5 ps remain very stable until the end of the simulation. This behavior is associated with the adsorbates staying on their initial adsorption sites, but vibrationally and rotationally (in the case of H_2^*) excited. Notice, however, that such a stable oscillatory behavior in ΔE_0, although related to direct adsorption events, is not a necessary condition because the possible anharmonicity and dephase among the multiple excited modes can mask the oscillations. The coexistence of multiple excited-modes also makes difficult to compare directly the $\Delta E_0(t)$ values with the energy diagram of Fig. 1.

In the case of the H*-embedding trajectory there is also a strong oscillatory behavior in ΔE_0 that accounts for the mobility of the adsorbates induced by H_2 adsorption (see Fig. 3, middle panels). However, at variance with the almost steady oscillations of the soft adsorption trajectories, we observe that the migration of H*(1) and H*(2) to positions below the five upper Pd atoms and their intercalation between Pd atoms, that occurs in the interval $t \simeq 1.0$–1.5 ps (black and red z_H curves in Fig. 3), is accompanied by a slight decrease in ΔE_0. This decrease seems to indicate that the embedding-type configurations reached by the

system are slightly more stable than the adsorbed configuration obtained by direct adsorption of H_2 on the available adsorption site of $9H_2^*$-Pd_6@Gvac without modification of the positions of the other H_2^* and H* adsorbates (shown in the second bottom panel of Fig. 1). Regarding the bent-cluster trajectory, Fig. 3 shows that the energy landscape probed during the adsorption process must be very different. Only on this kind of adsorbing trajectories there is a pronounced decrease of about 200 meV in ΔE_0 that contrasts with the more steady behavior exhibited by the two other types. Considering the complexity of the configurational space, it is difficult to determine the factors triggering the structural change. A common feature in the two bent trajectories seems to be the coincident intercalation of H*(4) and H*(5) between their respective nearest Pd neighbours, which occurs during the migration of the former to positions below the Pd-pentagon, and the large mobility of the nearby H_2^*. The driving force for this type of hydrogen dynamics on Pd_6 being that hydrogen is eager to interact strongly with palladium. Therefore, with increasing the hydrogen coverage of Pd_6, some H* atoms tend to migrate to the lower side of the cluster to strengthen their interaction with Pd. However, this kind of movements on the supported IPB-Pd_6 is hindered by steric effects of the graphene layer [68]. But for very high coverages of Pd_6 at or close to saturation, the concerted intercalation and migration to the lower part of Pd_6 of different H* atoms may induce the structural transformation of Pd_6 to an upwards bent configuration, thus avoiding the steric effect of the support and reaching more stable regions of the configurational space. This is the type of structural transformation observed in the two bent-cluster trajectories. The final hydrogen saturated bent-structure of Pd_6 is more stable than the saturated IPB-Pd_6 configuration formed at the early stages of the dynamics as the H_2 molecule collides with $9H_2^*$-Pd_6@Gvac, as it is clearly shown by the decrease in ΔE_0 (top right panel of Fig. 2). The bent configuration competes favourably with possible spillover configurations and H* migration to the graphene layer is not observed in any of the two bent-trajectories.

It is interesting to notice that both the H*-embedding and the bent-cluster trajectories show a favourable insertion of hydrogen in the Pd_6 cluster which can be considered as a precursor of the formation of solid Pd hydrides.

4.2. 0.125 eV-H_2 impinging on $9H_2^*$-Pd_6@Gvac at 300 K

In the AIMD simulations with the substrate at 300 K, H_2 adsorption occurs in 2 out of the 100 trajectories, which yields an adsorption probability similar to that at 0 K. In spite of this, there are significant differences between the two temperatures.

Warming up the $9H_2^*$-Pd_6@Gvac system to 300 K causes a strong mobility of all the adsorbates and the concomitant geometrical transformation of the initial IPB $9H_2^*$-Pd_6 structure. Fig. 4 shows a superposition of all the instantaneous positions of the adsorbates and Pd_6 cluster during the last 2.5 ps of the thermalization process, depicted on top of the equilibrium IPB $9H_2^*$-Pd_6 structure. The figure gives an idea of the ample configurational space that is probed at 300 K. The important difference with respect to 0 K is that H* and particularly H_2^*, being highly translationally excited at 300 K, are weakly bound to the cluster. As a result, adsorption of the incoming H_2 induces the desorption of one or more H_2^* molecules in both trajectories. This is what is observed in the snapshots of Fig. 5. The snapshots at $t = 75$ and 150 fs show that the adsorbing H_2 pushed down the nearby H_2^*, that ends up desorbing at $t = 225$ fs. The whole cluster is still so much perturbed that there is a second desorption event about one ps later. In fact, H_2^* desorption is also a common process in the scattering trajectories, suggesting that the mere interaction of gas-phase H_2 with the cluster at 300 K is enough to trigger the desorption process. It would also suggest that saturation of the Pd_6@Gvac at ambient temperature is limited to nine molecules at most. In order to get further evidence on this last conclusion, we performed a few additional simulations in which the IPB $10H_2^*$-Pd_6@Gvac system is simply thermalized at 300 K during 5 ps, following the same procedure that was used for $9H_2^*$-Pd_6@Gvac. There are three trajectories in five that show desorption of H_2^*. In the remaining two trajectories we observed a kind of frustrated desorption, all in all suggesting that the process is indeed very likely. This result is consistent with the work of Contescu et al. [42]. These workers found that by treating at 20°C for 24 h Pd-doped activated carbon fibers initially loaded with hydrogen at 77 K, most of the hydrogen desorbed into the gas phase.

Considering the strong mobility of all the adsorbates at 300 K, we might expect it would not only favor desorption but also H* migration to the graphene layer. However, none of the 100 AIMD trajectories and none of the five canonical AIMD trajectories show evidence for such a spillover process, even if there are adsorbates reaching heights over the carbon layer as close as 2.5 Å.

5. Discussion

The spillover mechanism has been often advocated to justify the enhancement of the hydrogen storage capacity of porous carbon materials induced by doping with palladium nanoparticles. In a previous work, we investigated the mechanism of hydrogen spillover from Pd clusters supported on pristine graphene (as a reasonable model for the pore walls) [45]. For this purpose, density functional molecular dynamics simulations were performed of the adsorption of molecular hydrogen on non-hydrogenated and hydrogenated Pd clusters. A large number of simulations were performed for Pd clusters of different sizes and different degrees of initial hydrogen coverage. A fraction of the impinging hydrogen molecules bounced back. The H_2 molecules that stick on the Pd clusters have a sizable probability of dissociating; that is, the Pd cluster catalyzes the H_2 dissociation, which is a key step in the spillover mechanism. However, out of a total of 240 simulations no sign of spillover of atomic or molecular hydrogen from the cluster towards the carbon substrate was detected. The fact that the Pd clusters were supported on pristine graphene made us uneasy because the metal clusters are usually attached to defects on the pore walls.

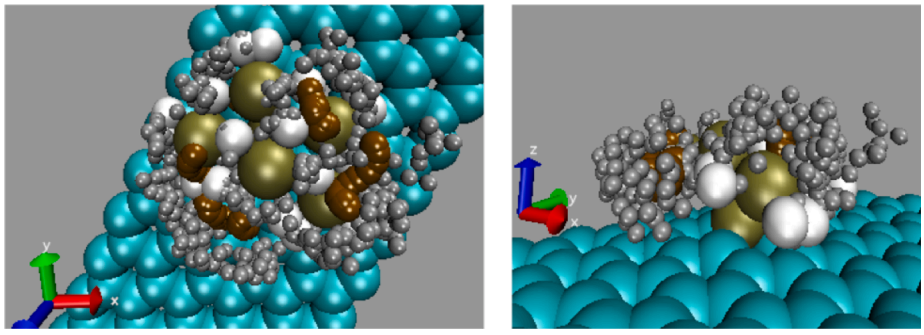

Fig. 4. Top (left) and side (right) views of the relaxed $9H_2^*$-Pd_6@Gvac system (large spheres: H in white, Pd in brown, and C in blue). Superimposed are shown the positions sampled in the time evolution of the H (small grey spheres) and Pd (small tan spheres) atoms during the last 2.5 ps of the simulated thermalization of $9H_2^*$-Pd_6@Gvac at 300 K. Thermalization positions are plotted using a time interval of 0.1 ps. The graphene movement is masked by the initial configuration. (For interpretation of the references to colour in this figure legend, the reader is referred to the web version of this article.)

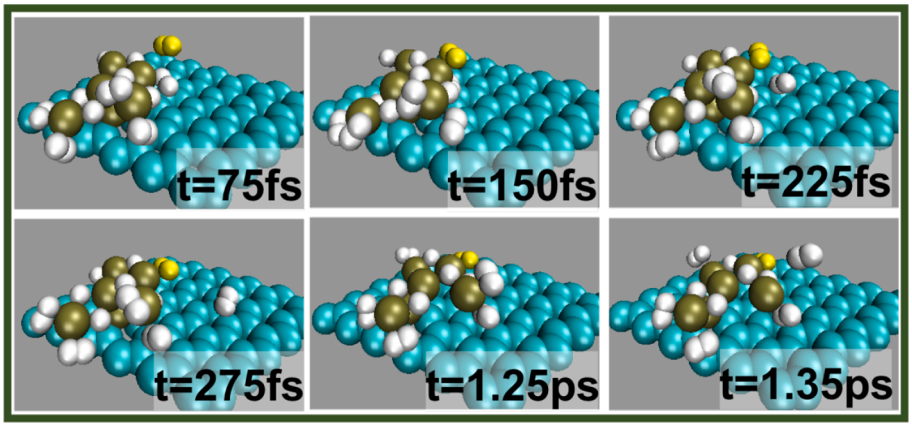

Fig. 5. Representative snapshots of one of the adsorbing AIMD trajectories that are identified at $T_s = 300$ K. Time interval indicated in each panel. White, blue, and brown spheres represent H, C, and Pd atoms. The adsorbing H_2 is colored in yellow. (For interpretation of the references to colour in this figure legend, the reader is referred to the web version of this article.)

On the other hand, saturation or near saturation hydrogen coverages that could be reached in experiments might facilitate the occurrence of spillover. For these reasons we have used more realistic conditions in the present work, namely, anchoring the metal clusters to graphene vacancies and using near saturation hydrogen coverages. First of all, anchored Pd clusters become well integrated in the pore wall. Second, in the particular case of Pd_6 investigated here, the structure of the cluster flattens substantially as a result of the dissociation of the adsorbed hydrogen molecules. In addition, the carbon atoms nearest to the vacancy have unsaturated dangling bonds and are reactive. These features led us to expect that the reactive C atoms could act as bridges to permit the spillover of H atoms towards the carbon substrate. In fact, the calculated DFT energies confirm that, for near hydrogen-saturated clusters, the configuration in which the H atoms are attached to those reactive C atoms is energetically favorable in comparison to configurations in which those H atoms are simply chemisorbed on the Pd cluster. After that, H migration from those locations to other more distant locations on the graphene layer would only cost an affordable amount of energy. Therefore, one would expect that the presence of defects and the conditions of hydrogen saturation or near saturation might facilitate the occurrence of spillover. However, in spite of these initial expectations the results of the ab initio molecular dynamics simulations do not support spillover. First, under the conditions of near saturation, adsorption of additional hydrogen becomes difficult and in most simulations the incoming molecules bounce back towards vacuum, often inducing the desorption of previously adsorbed molecules when the substrate is at room temperature. Furthermore, in the few cases in which the incoming molecules are adsorbed, new competitive structures enter into play having one or two H* atoms embedded within the Pd cluster. In some cases insertion of H* occurs on the IPB-Pd_6 configuration and, in others, it is accompanied by a structural transformation from IPB-Pd_6 towards an up-bent-Pd_6 configuration. However, no spillover occurs of the incoming adsorbed molecules or other previously adsorbed hydrogen atoms or molecules. Since spillover is not energetically forbidden, the explanation for the lack of spillover must be the existence of activation barriers high enough to prevent the migration of the H atoms towards the carbon substrate.

In order to confirm this hypothesis, we have performed additional calculations aimed to identify the possible magnitude of such barrier. From the AIMD simulations at 0 K, we found that the IPB $10H_2^*$-Pd_6@Gvac minimum energy configuration is achieved when one H* becomes embedded on the cluster. Thus, starting from this configuration, we calculate the energy cost of descending this embedded H* to the graphene layer. In searching for the minimum energy along this reaction coordinate Z_H, the (X,Y) position of the descending H*, as well as the (X, Y,Z) positions of, namely, the six Pd atoms in the cluster, the 13 C atoms around the vacancy, and the remaining 19 H* atoms, are optimized until the corresponding forces are below 0.1 eV/Å. Fig. 6 shows the corresponding minimum energy path together with images of selected configurations along the path. There is a high activation energy barrier of 0.621 eV that corresponds to locating H* at roughly 2.1 Å from the graphene layer. Once this critical distance is overpassed the energy decreases rapidly, as an indication of H* forming new bonds with the C atom below. The question that remains at this point is whether quantum effects can change the conclusions from our classical dynamics approach. In this respect, it is worthy to remark that the AIMD simulations already demonstrate that all the degrees of freedom involving the Pd cluster, the adsorbates, and the C atoms around the vacancy will play an important role, making a quantum treatment unfeasible nowadays. However, a meaningful alternative to quantum dynamics can be the semiclassical ring polymer molecular dynamics that has been successfully used to treat quantum effects in gas-phase reactions [69] and more recently in gas-surface dynamics [70,71]. Even if its applicability to this complex problem might be still demanding because of the large amount of degrees of freedom involved, one may think in applying it to explore at least the final stage of the migration process (Fig. 6). Nonetheless, it is worthy to note in this respect that a rough estimation on the tunnelling probability using the WKB approach and a simple triangular fit of the barrier, as done in Ref. [72] for H diffusion in bulk Pd, would suggest small tunneling probabilities in the order of 3×10^{-20} for H*located at the bottom of the well with the ZPE.

Finally, a few last remarks regarding our discussion on the likeliness of the spillover process and its connection to experiments are also in order. Pd_6 has been selected mainly because we can compare the calculations with previous ones with Pd_6 on a different support (pristine graphene). But there is nothing special in that size, which is viewed just as a representative small cluster. In practice, when porous carbons are doped with palladium, formation of metal clusters of different sizes is expected, and not a single size. The interaction of Pd atoms and clusters with defects in graphene is much stronger than the interaction with pristine graphene [47]. Then, in the process of doping porous carbons the diffusion of Pd atoms will stop at vacancies and other defects, and Pd clusters will easily form and become anchored at defects.

An argument often used to interpret the enhancement in the amount of hydrogen stored in Pd-doped porous carbons and carbon nanofibers is that the maximum amount of hydrogen absorbed in the metal nanoparticles is that corresponding to the stoichiometry of the solid hydride, $Pd_1H_{0.7}$; and that the rest is stored on the carbon surfaces after spillover. At least in the case of small Pd clusters this argument may need revision, because small clusters are more reactive and have a sizeable surface/volume ratio. We have seen that a Pd_6 cluster anchored to a graphene vacancy can store ten hydrogen molecules (some of them dissociated),

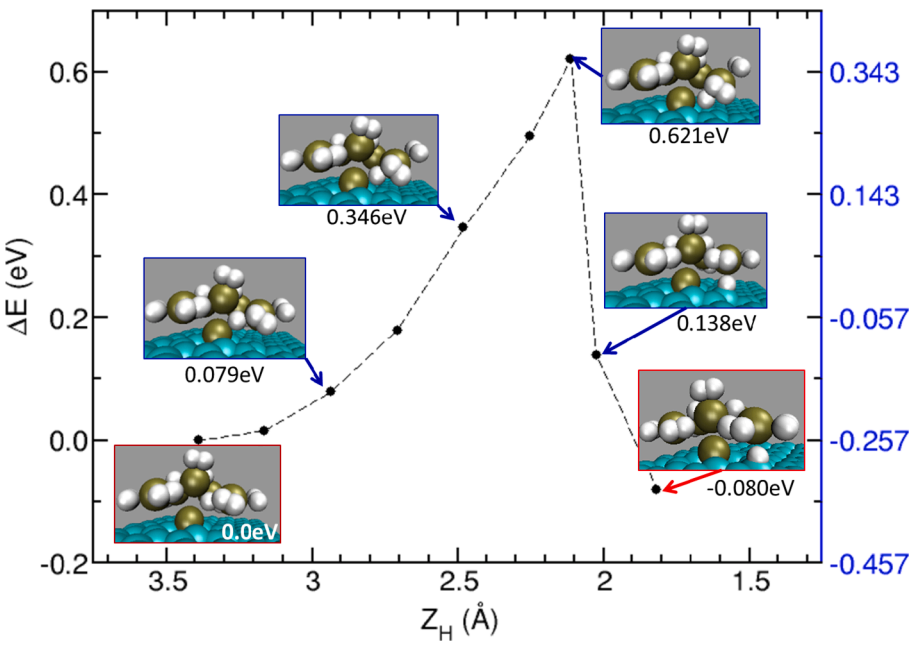

Fig. 6. Minimum energy path to descend from the H* embedded position (first image) to the H*-migration-2 configuration on the graphene layer (see Fig. 1). Energies ΔE on the left axis are referred to the initial H* embedded configuration. The values respect to the gas-phase H_2 and $9H_2^*$-Pd_6@Gvac system, i.e., the zero energy in Fig. 1, are shown in the right blue axis. White, blue, and brown spheres represent H, C, and Pd atoms. (For interpretation of the references to colour in this figure legend, the reader is referred to the web version of this article.)

which gives a very different $Pd_1H_{3.3}$ stoichiometry.

6. Conclusions

Ab initio density functional molecular dynamics (AIMD) simulations of the low energy deposition of molecular hydrogen on hydrogenated Pd_6 clusters anchored on graphene vacancies (Gvac) have been performed. The anchored palladium clusters are initially near-saturated with hydrogen. Five hundred simulations have been run in which the hydrogenated Pd_6@Gvac substrate is initially at a temperature of 0 K, and one hundred simulations with the substrate initially at 300 K. The purpose of the AIMD simulations has been double. One objective was to analyze the process of full saturation of the Pd cluster with hydrogen. Achieving full saturation when the cluster is already near saturated becomes difficult, because many incoming H_2 molecules bounce back to vacuum and even can induce the desorption of one or more of the previously adsorbed H_2 molecules when the substrate is at room temperature. Moreover, our AIMD simulations show that at very high coverages at or near saturation, adsorbed H atoms tend to embed into the Pd cluster inducing in some cases profound structural transformations. The second, and more important objective, was to investigate the effectiveness of the mechanism of hydrogen spillover, usually advocated to interpret the observed enhancement of the hydrogen storage capacity in porous carbon materials doped with metal nanoparticles. Although the process is energetically exothermic for the system and conditions investigated here, the AIMD simulations reveal that high activation barriers exist preventing in practice the spillover of adsorbed hydrogen atoms from the anchored Pd cluster towards the carbon substrate.

Declaration of Competing Interest

The authors declare that they have no known competing financial interests or personal relationships that could have appeared to influence the work reported in this paper.

Acknowledgement

The authors acknowledge financial support by the Gobierno Vasco-UPV/EHU Project No. IT1246-19, the Spanish Ministerio de Ciencia e Innovación [Grants No. PID2019-107396 GB-I00/AEI/10.13039/501100011033 and PID2019-104924RB-I00], Junta de Castilla y León [Grant VA021G18], and University of Valladolid (Grupo de Física de Nanoestructuras). A. G. acknowledges a predoctoral fellowship from Junta de Castilla y León. The authors thankfully acknowledge the facilities provided by Centro de Proceso de Datos-Parque Científico (University of Valladolid) and by the DIPC computing center. The use of the VMD software [73] to produce some of the figures is also acknowledged.

References

[1] J.M. Ogden, Hydrogen: The fuel of the future? Phys. Today 55 (4) (2002) 69–75.
[2] G.W. Crabtree, M.S. Dresselhaus, M.V. Buchanan, The hydrogen economy, Phys. Today 57 (12) (2004) 39–44.
[3] P. Jena, Materials for hydrogen storage: Past, present, and future, J. Phys. Chem. Lett. 2 (2011) 206–211.
[4] Fuel Cell Handbook, 7th Edition, EG&G Services Inc., US DOE, Morgantown, WV, 2004.
[5] Target explanation document: Onboard hydrogen storage for light-duty fuel cell vehicles. us doe (2017).
[6] S. Patchkovskii, J.S. Tse, S.N. Yurchenko, L. Zhechkov, T. Heine, G. Seifert, Graphene nanostructures as tunable storage media for molecular hydrogen, Proc. Natl. Acad. Sci. USA 10439–10444 (2005).
[7] G. Yushin, R. Dash, J. Jagiello, J.E. Fisher, Y. Gogotsi, Carbide-derived carbons: Effect of pore size on hydrogen uptake and heat of adsorption, Adv. Funct. Mater. 16 (2006) 2288–2293.
[8] I. Cabria, M.J. López, J.A. Alonso, Simulation of the hydrogen storage in nanoporous carbons with different pore shapes, Int. J. Hydrogen Energy 36 (2011) 10748–10759.
[9] J.A. Alonso, I. Cabria, M.J. López, Simulation of hydrogen storage in porous carbons, J. Mater. Res. 28 (2013) 589–604.
[10] R. Ströbel, J. Garche, P. Moseley, L. Jörissen, G. Wolf, Hydrogen storage by carbon materials, J. Power Sources 159 (2006) 781–801.
[11] A.G. Wong-Foy, A.J. Matzger, O.M. Yaghi, Exceptional h_2 saturation uptake in microporous metal-organic frameworks, J. Am. Chem. Soc. 128 (2006) 3494–3495.
[12] H. Langmi, A. Walton, M. Al-Mamouri, S. Johnson, D. Book, J. Speight, P. Edwards, I. Gameson, P. Anderson, I. Harris, Hydrogen adsorption in zeolites a, x, y and rho, J. Alloys Compd. 356–357 (2003) 710–715.
[13] W.L. Mao, H.-K. Mao, A.F. Goncharov, V.V. Struzhkin, Q. Guo, J. Hu, J. Shu, R. J. Hemley, M. Somayazulu, Y. Zhao, Hydrogen clusters in clathrate hydrate, Science 297 (2002) 2247–2249.
[14] N.B. McKeown, P.M. Budd, D. Book, Microporous polymers as potential hydrogen storage materials, Macromol. Rapid Commun. 28 (2007) 995–1002.
[15] A. Laikhtman, S. Michaelson, A. Hoffman, T.K. Kim, H.R. Moon, A. Zak, Using hydrogen activated by microwave plasma vs. molecular hydrogen for hydrogen storage in tungsten disulfide inorganic nanotubes, Int. J. Hydrogen Energy 39 (2014) 9837–9841.
[16] A. Laikhtman, G. Makrinich, M. Sezen, M.M. Yildizhan, J.I. Martínez, D. Dinescu, M. Prodana, M. Enachescu, J.A. Alonso, A. Zak, Hydrogen chemical configuration

and thermal stability in tungsten disulfide nanoparticles exposed to hydrogen plasma, J. Phys. Chem. C 121 (2017) 10747–10756.
[17] P. Chen, X. Wu, J. Lin, K.L. Tan, High h_2 uptake by alkali-doped carbon nanotubes under ambient pressure and moderate temperatures, Science 285 (1999) 91–93.
[18] R.T. Yang, Hydrogen storage by alkali-doped carbon nanotubes revisited, Carbon 38 (2000) 623–626.
[19] N. Alam, R. Mokaya, The effect of al content of zeolite template on the properties and hydrogen storage capacity of zeolite templated carbons, Micropor. Mesopor. Matter. 144 (2011) 140–147.
[20] V. Tozzini, V. Pellegrini, Prospects for hydrogen storage in graphene, Phys. Chem. Chem. Phys. 15 (2013) 80–89.
[21] A.D. Lueking, R.T. Yang, Hydrogen spillover to enhance hydrogen storage-study of the effect of carbon physicochemical properties, Appl. Catal. A 265 (2004) 259–268.
[22] E. Yoo, L. Gao, T. Komatsu, N. Yagai, K. Arai, T. Yamazaki, K. Matsuishi, T. Matsumoto, J. Nakamura, Atomic hydrogen storage in carbon nanotubes promoted by metal catalysts, J. Phys. Chem. B 108 (2004) 18903–18907.
[23] R. Zacharia, K.Y. Kim, A.F.F. Kibria, K.S. Nahm, Enhancement of hydrogen storage capacity of carbon nanotubes via spillover from vanadium and palladium nanoparticles, Chem. Phys. Lett. 412 (2005) 369–375.
[24] G.Q.A.J. Lachawiec, R.T. Yang, Hydrogen storage in nanostructured carbons by spillover: Bridge-building enhancement, Langmuir 21 (2005) 11418–11424.
[25] B.-J. Kim, Y.-S. Lee, S.-J. Park, Preparation of platinum-decorated porous graphite nanofibers, and their hydrogen storage behaviors, J. Colloid Interface Sci. 318 (2008) 530–533.
[26] V.V. Bhat, C.I. Contescu, N.C. Gallego, F.S. Baker, Atypical hydrogen uptake on chemically activated, ultramicroporous carbon, Carbon 48 (5) (2010) 1331–1340.
[27] C.I. Contescu, K. van Benthem, S. Li, C.S. Bonifacio, S.J. Pennycook, P. Jena, N. C. Gallego, Single pd atoms in activated carbon fibers and their contribution to hydrogen storage, Carbon 49 (2011) 4050–4058.
[28] S.Z. Mortazavi, P. Parvin, A. Reyhani, R. Malekfar, S. Mirershadi, Hydrogen storage property of laser induced pd-nanoparticle decorated multi-walled carbon nanotubes, RSC Adv. 3 (2013) 1397–1409.
[29] K. Wenelska, B. Michalkiewicz, J. Gong, T. Tang, R. Kaleczuk, X. Chen, E. Mijowska, In situ deposition of pd nanoparticles with controllable diameters in hollow carbon spheres for hydrogen storage, Int. J. Hydrogen Energy 38 (2013) 16179–16184.
[30] P. Divya, S. Ramaprabhu, Hydrogen storage in platinum decorated hydrogen exfoliated graphene sheets by spillover mechanism, Phys. Chem. Chem. Phys. 16 (2014) 26725–26729.
[31] R. Kumar, J.-H. Oh, H.-J. Kim, J.-H. Jung, C.-H. Jung, W.G. Hong, H.-J. Kim, J.-Y. Park, I.-K. Oh, Nanohole-structured and palladium-embedded 3d porous graphene for ultrahigh hydrogen storage and co oxidation multifunctionalities, ACS Nano 9 (2015) 7343–7351.
[32] C. Zhou, J.A. Szpunar, X. Cui, Synthesis of ni/graphene nanocomposite for hydrogen storage, ACS Appl. Matter Interfaces 8 (2016) 15232–15241.
[33] B. Zielinska, B. Michalkiewicz, X. Chen, E. Mijowska, R.J. Kalenczuk, Pd supported ordered mesoporous hollow carbon spheres OMHCS for hydrogen storage, Chem. Phys. Lett. 647 (2016) 14–19.
[34] W. Conner, J. Falconer, Spillover in heterogeneous catalysis, Chem. Rev. 95 (1995) 759–788.
[35] H. Cheng, L. Chen, A.C. Cooper, X. Sha, G.P. Pez, Hydrogen spillover in the context of hydrogen storage using solid-state materials, Energy Environ. Sci. 1 (2008) 338–354.
[36] R. Prins, Hydrogen spillover. facts and fiction, Chem. Rev. 112 (2012) 2714–2738.
[37] W. Karim, C. Spreafico, A. Kleibert, J. Gobrecht, J. VandeVondele, Y. Ekinci, J. A. van Bokhoven, Catalyst support effects on hydrogen spillover, Nature 541 (2017) 68–71.
[38] V.B. Parambhath, R. Nagar, S. Ramaprabhu, Effect of nitrogen doping on hydrogen storage capacity of palladium decorated graphene, Langmuir 28 (2012) 7826–7833.
[39] L. Chen, A.C. Cooper, G.P. Pez, H. Cheng, Mechanistic study on hydrogen spillover onto graphitic carbon materials, J. Phys. Chem. C 111 (2007) 18995–19000.
[40] W. Karim, A. Kleibert, U. Hartfelder, A. Balan, J. Gobrecht, J.A. van Bokhoven, Y. Ekinci, Size-dependent redox behavior of iron observed by in-situ single nanoparticle spectro-microscopy on well-defined model systems, Sci. Rep. 6 (2016) 18818.
[41] C. Bores, I. Cabria, J.A. Alonso, M.J. López, Adsorption and dissociation of molecular hydrogen on the edges of graphene nanoribbons, J. Nanoparticle Res. 14 (12) (2012) 1263.
[42] C.I. Contescu, C.M. Brown, Y. Liu, V.V. Bhat, N.C. Gallego, Detection of hydrogen spillover in palladium-modified activated carbon fibers during hydrogen adsorption, J. Phys. Chem. C 113 (2009) 5886–5890.
[43] M.J. López, I. Cabria, J.A. Alonso, Simulated porosity and electronic structure of nanoporous carbons, J. Chem. Phys. 135 (104706) (2011) 1–9.
[44] C. de Tomás, I. Suarez-Martinez, F. Vallejos-Burgos, M.J. López, K. Kaneko, N. A. Marks, Structural prediction of graphitization and porosity in carbide-derived carbons, Carbon 119 (2017) 1–9.
[45] M. Blanco-Rey, J.I. Juaristi, M. Alducin, M.J. López, J.A. Alonso, Is spillover relevant for hydrogen adsorption and storage in porous carbons doped with palladium nanoparticles? J. Phys. Chem. C 120 (31) (2016) 17357–17364.
[46] R.E. Palmer, S. Pratontep, H.G. Boyen, Nanostructured surfaces from size-selected clusters, Nature Mat. 2 (2003) 443–448.
[47] M.J. López, I. Cabria, J.A. Alonso, Palladium Clusters Anchored on Graphene Vacancies and Their Effect on the Reversible Adsorption of Hydrogen, J. Phys. Chem. C 118 (2014) 5081–5090.
[48] M. Alducin, J.I. Juaristi, A. Granja-DelRío, M.J. López, J.A. Alonso, Dynamics of cluster isomerization induced by hydrogen adsorption, J. Phys. Chem. C 123 (24) (2019) 15236–15243.
[49] W. Kohn, L.J. Sham, Self-consistent equations including exchange and correlation effects, Phys. Rev. 140 (1965) A1133–A1138.
[50] G. Kresse, J. Furthmüller, Efficiency of ab-initio total energy calculations for metals and semiconductors using a plane-wave basis set, Compt. Mater. Sci. 6 (1) (1996) 15–50.
[51] G. Kresse, J. Hafner, Ab initio molecular dynamics for liquid metals, Phys. Rev. B 47 (1993) 558–561.
[52] J.P. Perdew, J.A. Chevary, S.H. Vosko, K.A. Jackson, M.R. Pederson, D.J. Singh, C. Fiolhais, Atoms, molecules, solids, and surfaces: Applications of the generalized gradient approximation for exchange and correlation, Phys. Rev. B 46 (1992) 6671–6687.
[53] A. Granja, J.A. Alonso, I. Cabria, M.J. López, Competition between Molecular and Dissociative Adsorption of Hydrogen on Palladium Clusters Deposited on Defective Graphene, RSC Advances 5 (2015) 47945–47953.
[54] I. Cabria, M.J. López, S. Fraile, J.A. Alonso, Adsorption and dissociation of molecular hydrogen on palladium clusters supported on graphene, J. Phys. Chem. C 116 (2012) 21179–21189.
[55] P.E. Blöchl, Projector augmented-wave method, Phys. Rev. B 50 (1994) 17953–17979.
[56] G. Kresse, D. Joubert, From ultrasoft pseudopotentials to the projector augmented-wave method, Phys. Rev. B 59 (1999) 1758–1775.
[57] H.J. Monkhorst, J.D. Pack, Special points for brillouin-zone integrations, Phys. Rev. B 13 (1976) 5188–5192.
[58] M. Methfessel, A.T. Paxton, High-precision sampling for brillouin-zone integration in metals, Phys. Rev. B 40 (1989) 3616–3621.
[59] S. Nosé, A unified formulation of the constant temperature molecular dynamics methods, J. Chem. Phys. 81 (1) (1984) 511–519.
[60] D. Novko, I. Lončarić, M. Blanco-Rey, J.I. Juaristi, M. Alducin, Energy loss and surface temperature effects in ab initio molecular dynamics simulations: N adsorption on ag(111) as a case study, Phys. Rev. B 96 (2017) 085437.
[61] A. Groß, A. Dianat, Hydrogen dissociation dynamics on precovered pd surfaces: Langmuir is still right, Phys. Rev. Lett. 98 (2007) 206107.
[62] F. Nattino, C. Díaz, B. Jackson, G.-J. Kroes, Effect of surface motion on the rotational quadrupole alignment parameter of $\mathbf{d}_2$ reacting on cu(111), Phys. Rev. Lett. 108 (2012) 236104.
[63] F. Nattino, H. Ueta, H. Chadwick, M.E. van Reijzen, R.D. Beck, B. Jackson, M.C. van Hemert, G.-J. Kroes, Ab initio molecular dynamics calculations versus quantum-state-resolved experiments on chd3 + pt(111): New insights into a prototypical gas surface reaction, J. Phys. Chem. Lett. 5 (8) (2014) 1294–1299, pMID: 26269970.
[64] B. Kolb, H. Guo, Communication: Energy transfer and reaction dynamics for dcl scattering on au(111): An ab initio molecular dynamics study, J. Chem. Phys. 145 (1) (2016) 011102.
[65] X. Zhou, B. Kolb, X. Luo, H. Guo, B. Jiang, Ab initio molecular dynamics study of dissociative chemisorption and scattering of co2 on ni(100): Reactivity, energy transfer, steering dynamics, and lattice effects, J. Phys. Chem. C 121 (10) (2017) 5594–5602.
[66] L. Zhou, B. Jiang, M. Alducin, H. Guo, Communication: Fingerprints of reaction mechanisms in product distributions: Eley-rideal-type reactions between d and cd3/cu(111), J. Chem. Phys. 149 (3) (2018) 031101.
[67] G. Füchsel, X. Zhou, B. Jiang, J.I. Juaristi, M. Alducin, H. Guo, G.-J. Kroes, Reactive and nonreactive scattering of hcl from au(111): An ab initio molecular dynamics study, J. Phys. Chem. C 123 (4) (2019) 2287–2299.
[68] A. Granja-DelRío, J.A. Alonso, M.J. López, Steric and chemical effects on the hydrogen adsorption and dissociation on free and graphene-supported palladium clusters, Computational and Theoretical Chemistry 1107 (2017) 23–29.
[69] S. Habershon, D.E. Manolopoulos, T.E. Markland, T.F. Miller, Ring-polymer molecular dynamics: Quantum effects in chemical dynamics from classical trajectories in an extended phase space, Annu. Rev. Phys. Chem. 64 (1) (2013) 387–413, pMID: 23298242.
[70] Y.V. Suleimanov, Surface diffusion of hydrogen on ni(100) from ring polymer molecular dynamics, J. Phys. Chem. C 116 (20) (2012) 11141–11153.
[71] Q. Liu, L. Zhang, Y. Li, B. Jiang, Ring polymer molecular dynamics in gasâ€"surface reactions: Inclusion of quantum effects made simple, J. Phys. Chem. Lett. 10 (23) (2019) 7475–7481, pMID: 31738557.
[72] M. Blanco-Rey, M. Alducin, J.I. Juaristi, P.L. de Andres, Diffusion of hydrogen in pd assisted by inelastic ballistic hot electrons, Phys. Rev. Lett. 108 (2012) 115902.
[73] W. Humphrey, A. Dalke, K. Schulten, VMD – Visual Molecular Dynamics, J. Mol. Graph. 14 (1996) 33–38.